Paleoceanography and Paleoclimatology

RESEARCH ARTICLE
10.1029/2017PA003309

Key Points:
- We present the first record of fish teeth and sedimentary coating neodymium isotopes from the abyssal Philippine Sea (North Pacific) during the Neogene
- This Deep Pacific water mass shifted from a North Pacific source in the Early Miocene to a southern source by ~14 Ma
- This major reorganization of North Pacific water mass structure may have been linked with Antarctic glaciation of the middle Miocene climate transition

Correspondence to:
S. Kender,
s.kender@exter.ac.uk

Citation:
Kender, S., Bogus, K. A., Cobb, T. D., & Thomas, D. J. (2018). Neodymium evidence for increased circumpolar deepwater flow to the North Pacific during the middle Miocene climate transition. *Paleoceanography and Paleoclimatology*, *33*. https://doi.org/10.1029/2017PA003309

Received 17 DEC 2017
Accepted 4 JUN 2018
Accepted article online 11 JUN 2018

Neodymium Evidence for Increased Circumpolar Deep Water Flow to the North Pacific During the Middle Miocene Climate Transition

Sev Kender[1,2], Kara A. Bogus[1,3], Ty D. Cobb[4], and Deborah J. Thomas[4]

[1]Camborne School of Mines, University of Exeter, Penryn, UK, [2]British Geological Survey, Keyworth, Nottingham, UK, [3]International Ocean Discovery Program, Texas A&M University, College Station, TX, USA, [4]Department of Oceanography, Texas A&M University, College Station, TX, USA

Abstract Low salinity surface water inhibits local deepwater formation in the modern North Pacific. Instead, southern-sourced Circumpolar Deep Water (CDW) fills the basin, which is the product of water masses formed from cold sinking centers in the Southern Ocean and North Atlantic. This CDW is responsible for transporting a significant amount of global heat and dissolved carbon in the deep Pacific Ocean. The history of its flow and the broader overturning circulation are widely assumed to be sensitive to climate perturbations. However, insufficient records exist of CDW presence in the deep North Pacific with which to evaluate its evolution and role in major climate transitions of the past 23 Ma. Here we report sedimentary coatings and fish teeth neodymium isotope values—tracers for water-mass mixing—from deepwater International Ocean Discovery Program Site U1438 (4.7 km water depth) in the Philippine Sea, northwest Pacific Ocean. Our results indicate the water mass shifted from a North Pacific source in the early Miocene to a southern source by ~14 Ma. Within the age model and temporal constraints, this major reorganization of North Pacific water mass structure may have coincided with ice sheet build up on Antarctica and is most consistent with an increased northward flux of CDW due to enhanced sinking of cold water forced by Antarctic cooling. The northward extent of this flux may have remained relatively constant during much of the past 14 Ma.

1. Introduction

Overturning circulation in the modern Pacific Ocean is driven by Circumpolar Deep Water (CDW), which is sourced from cold sinking centers around Antarctica and the North Atlantic (Ferrari et al., 2014; Talley, 2013; Talley et al., 2011). Low surface water density in the North Pacific precludes significant local convection, and Pacific meridional overturning circulation (PMOC) is sluggish compared with the Atlantic (Ferrari et al., 2014; Kawabe & Fujio, 2010). As CDW enters the Pacific at depth, it travels northward (Figure 1), gradually exchanging with intermediate water before flowing back to the Southern Ocean as North Pacific Deep Water (NPDW, sometimes referred to as Pacific Central Water) between 1 and 3 km depth (Kawabe & Fujio, 2010). Thus, CDW transports heat and dissolved carbon into the deep North Pacific, forming a major carbon reservoir separated from the atmosphere (Ferrari et al., 2014). Changes in PMOC have the potential to impact global temperature, moisture supply, and the carbon cycle, and there have been several attempts to reconstruct PMOC over the Cenozoic to understand its past roles in climate change and tectonic evolution (e.g., Butzin et al., 2011). In particular, it is not yet known how PMOC responded to major climate transitions such as the middle Miocene climate transition (MMCT, ~14 Ma).

Several neodymium (Nd) isotope and modeling studies have shown that the Pacific was characterized by local overturning in the north as well as the south during much of the warmest intervals in the Paleogene, with a major shift toward southern-sourced deep water in the north after ~40 Ma (e.g., Thomas, 2004; Thomas et al., 2014). Modeling studies have suggested that Oligocene and Miocene ocean circulation was different to present, with a higher salinity North Pacific due to an open Panama Strait and, perhaps in some ways similar to the Paleogene, with possible local deepwater formation in the North (Butzin et al., 2011; von der Heydt & Dijkstra, 2006). However, currently, there is a large data set gap with no water mass records from the deep North Pacific with which to ascertain changes to the northward extent of CDW or local overturning during the past 23 Ma. Existing North Pacific Nd isotope records from the Neogene are restricted to intermediate water (<3 km depth) sites and deep (>5 km) central and South Pacific sites (Holbourn et al., 2013; Le Houedec et al., 2016; Ling et al., 1997; Martin & Haley, 2000; van de Flierdt et al., 2004). These records

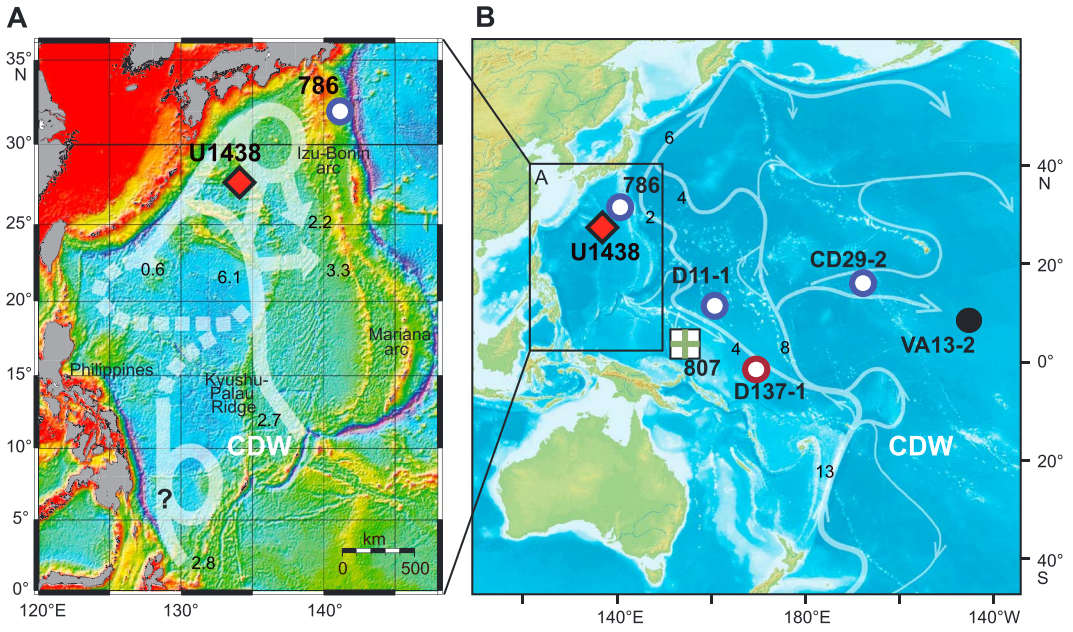

Figure 1. Bathymetric location maps of core sites and major ocean currents. (a) Bathymetric map of the Philippine Sea with location of IODP Site U1438 (red diamond; this study) and ODP Site 786 (blue circle). Modern Ocean currents are shown for bottom water around 4,000 m (45.845 isobath; Kaneko et al., 2001), here referred to as Circumpolar Deep Water (CDW). Numbers refer to Sv (volume water flow per second). The dashed lines and question marks denote uncertainty. (b) Bathymetric map of the Pacific Ocean, with locations of sites discussed in the text, and the regional path of lower CDW influence centered around 4,500-m water depth (Kawabe & Fujio, 2010).

exhibit an approximately unchanging isotopic offset from each other with depth throughout the Neogene, attesting that there were distinct water mass signatures somewhat similar to today (van de Flierdt et al., 2004). They show a long-term trend of gradually more radiogenic values at all depths from ~20–3 Ma, suggested to be the result of the Isthmus of Panama closure (Bartoli et al., 2005; Duque-Caro, 1990) gradually cutting off the supply of nonradiogenic Atlantic water into the Pacific (Duque-Caro, 1990; Martin & Haley, 2000). Alternatively, gradual Pacific Plate movement transporting all sites toward more proximal volcanic centers in the West Pacific has been suggested by Le Houedec et al. (2016), but we note that western sites do not show more radiogenic values than eastern sites of a similar water depth (e.g., Sites D11-1 and CD29-2 have similar values; Ling et al., 1997).

To address this data set gap and gain insights into deep ocean circulation dynamics of the Neogene, we measured the Nd isotopic values of fossil fish teeth and ferromanganese oxyhydroxide coatings as a water-mass tracer from IODP Site U1438 (Figure 1) in the Philippine Sea, NW Pacific (Arculus, Ishizuka, Bogus, & Expedition 351 Scientists, 2015; Arculus, Ishizuka, Bogus, Gurnis, et al., 2015), over the past 23 Ma. The site is located at 4.7 km depth and is currently bathed in CDW.

2. Materials and Methods

2.1. Site U1438

In 2014, IODP Expedition 351 cored Site U1438 (Arculus, Ishizuka, Bogus, & Expedition 351 Scientists, 2015). The lithology of Site U1438 consists of pelagic noncalcareous abyssal clays with discrete tephra layers and dust in the top ~160 m (Unit I, 26 Ma to Holocene), transitioning below into coarser grained tuffaceous muds and sands that continue down to ~305 m (Unit II, 29 to 26 Ma). The age model is robust, with nearly all paleomagnetic reversals present, and tied to radiolarian biostratigraphy in the middle Miocene (~15 Ma) and nannofossil biostratigraphy in the late Oligocene (at 27 Ma; Arculus, Ishizuka, Bogus, & Expedition 351 Scientists, 2015; Figure 2).

Site U1438, currently at 4.7 km water depth, has been situated below the carbonate compensation depth (CCD) for the past 26 Ma (modern CCD depth ~4.5 km) based on the lack of carbonate throughout the

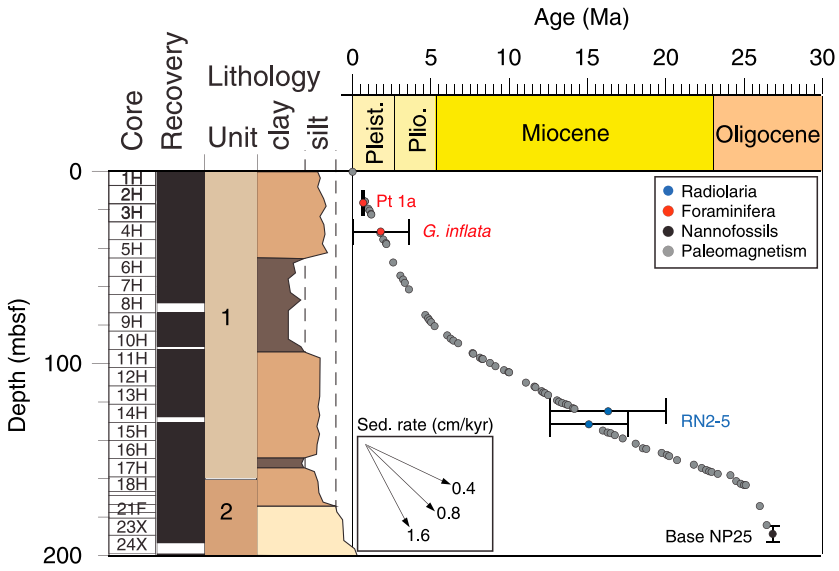

Figure 2. Age model for Site U1438, showing the position of paleomagnetic reversals (gray circles) and biostratigraphic data (red = planktonic foraminifera; blue = radiolaria; black = calcareous nannofossils). The lithological color refers to average grain size. See Arculus, Ishizuka, Bogus, and Expedition 351 Scientists (2015) for further details.

whole of Unit I (<0.5 wt%; Arculus, Ishizuka, Bogus, & Expedition 351 Scientists, 2015). The CCD has been constrained to deeper than 4.5 km throughout the Oligocene and Miocene in the equatorial Pacific (Pälike et al., 2012), indicating that Site U1438 was monitoring >4.5 km water depth for the duration of our 23 Ma record. The Philippine Sea Plate, upon which Site U1438 is located, was in a position about 6° southward of its current location at ~20 Ma (Richter & Ali, 2015; Wu et al., 2016) and has rotated steadily northward since then (Figure 3).

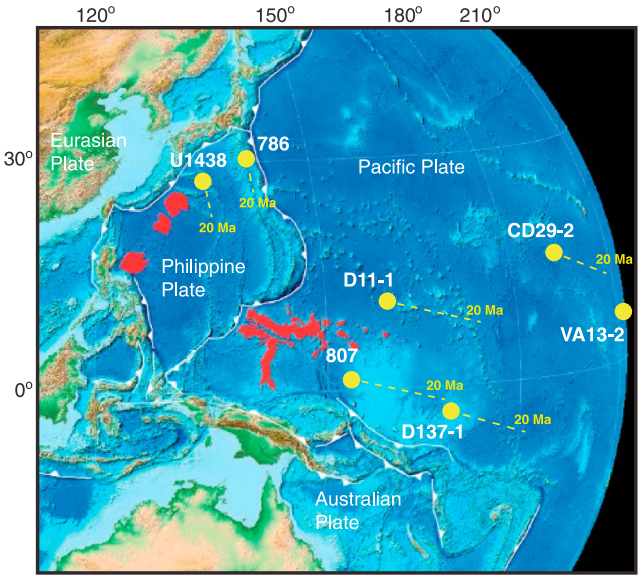

Figure 3. Bathymetric map showing the current position of Site U1438 (this study) and other sites referred to in the text (yellow circles) and reconstructed approximate site positions at 20 Ma relative to the Eurasian Plate (based on plate reconstructions from Wu et al., 2016). The white lines indicate plate boundaries. The red areas are various hot spot sites active before 30 Ma (Ishizuka et al., 2013). For details of plate reconstruction methods see Wu et al. (2016).

2.2. Use of Nd Isotopes as a Water Mass Tracer

Dissolved Nd is a robust tracer of water-mass composition owing in part to its short residence time (~0.3–1 ka, Tachikawa et al., 2003) relative to oceanic mixing (~1.5 ka). Seawater Nd isotope ratios ($^{143}Nd/^{144}Nd$ normalized to bulk Earth, expressed as ε_{Nd}, De Paolo & Wasserburg, 1976) are different in each of the modern ocean basins, as ε_{Nd} varies depending on the source region of fluvial discharge, boundary exchange, and dust sources (Arsouze et al., 2007; Jones et al., 1994; Wilson et al., 2013). The North Pacific is surrounded by geologically radiogenic sources, and thus, shallow waters have highly radiogenic values (−2), while underlying water is less radiogenic because of the influence of deeper waters from the Southern Ocean (−8). Therefore, North Pacific Deep Water has a somewhat elevated signature (−5) due to gradual exchange with intermediate water, resulting in a reduced but robust ε_{Nd} gradient that is clearly shown in water column measurements (Amakawa et al., 2009) but has proved challenging to model (Arsouze et al., 2007). One complication with reconstructing water masses is the radiogenic pore water flux detected in marginal settings, such as the Oregon Margin (Abbott et al., 2015) and Gulf of Alaska (Haley et al., 2014) up to ~100 km from the shelf, where seawater ε_{Nd} at least in the top 3.5 km water depth is elevated above more typical open ocean Pacific values.

2.3. Analytical Procedures

We reconstructed past water mass signatures at Site U1438 by measuring ε_{Nd} of fossil fish teeth and ferromanganese oxyhydroxide coatings,

Table 1
Site U1438 Nd Isotope Data From Fossil Fish Teeth

Core	Section	Depth (mbsf)	Age (Ma)	$^{143}Nd/^{144}Nd$	Std. error (abs)	ε_{Nd} (t)	
1H	4	2.90	0.15	0.512447	0.000008	−3.7±	0.3
3H	4	22.60	1.20	0.512405	0.000009	−4.5±	0.3
4H	4	32.10	1.76	0.512445	0.000006	−3.8±	0.2
4H	CC	35.73	1.98	0.512443	0.000003	−3.7±	0.1
5H	4	41.60	2.32	0.512458	0.000004	−3.5±	0.2
5H	CC	44.89	2.47	0.512444	0.000003	−3.8±	0.1
7H	4	60.60	3.54	0.512451	0.000007	−3.6±	0.3
7H	CC	64.09	3.81	0.512469	0.000002	−3.3±	0.1
7H	CC	64.09	3.81	0.512491	0.000012	−2.8±	0.5
8H	2	67.07	4.05	0.512503	0.000009	−2.6±	0.3
8H	3	68.58	4.16	0.512444	0.000006	−3.7±	0.2
9H	4	79.60	5.14	0.512461	0.000005	−3.4±	0.2
10H	2	85.00	6.00	0.512411	0.000003	−4.4±	0.1
11H	7	102.17	9.31	0.512416	0.000003	−4.3±	0.1
12H	4	108.05	10.69	0.512417	0.000003	−4.2±	0.1
12H	CC	111.97	11.63	0.512384	0.000010	−4.9±	0.4
13H	4	117.55	12.73	0.512502	0.000006	−2.6±	0.2*
13H	4	117.55	12.73	0.512398	0.000006	−4.6±	0.2
13H	CC	121.37	13.69	0.512385	0.000004	−4.8±	0.2
15H	4	136.42	16.49	0.512417	0.000007	−4.2±	0.3
15H	CC	139.64	17.49	0.512415	0.000008	−4.2±	0.3
15H	CC	139.64	17.49	0.512416	0.000004	−4.2±	0.2
16H	CC	148.96	20.40	0.512427	0.000009	−4.0±	0.4
17H	5	157.05	23.23	0.512456	0.000005	−3.4±	0.2

*Data point not shown on Figure 5 after repeating. It is assumed reworked or possibly affected by dispersed ash.

which record the isotopic value of bottom water at the sediment surface (Reynard et al., 1999). The fossil fish teeth and teeth debris collected from Site U1438 sediment samples were prepared using the general methods of Basak et al. (2011) and Xie et al. (2012). To isolate the teeth/debris, bulk sediment was disaggregated and washed over a 63-μm sieve. The retained material was dried overnight in an oven (50°C). For analysis, approximately 15–30 specimens per sample were handpicked using a binocular microscope and fine brush. The specimens were then washed 3 times with ultrapure water (Milli-Q).

For Fe-Mn oxyhydroxide coating analysis, bulk samples were dried overnight and were subsequently pulverized and homogenized with an agate mortar and pestle. These homogenized samples were decarbonated for 2 hr using sodium acetate buffered acetic acid solution that was precleaned in cation exchange resin. The remaining material was washed 3 times with Milli-Q. To reduce the Fe-Mn phases, the oxide fraction was

Table 2
Site U1438 Nd Isotope Data From Fe-Mn Oxyhydroxide Coatings

Core	Section	Depth (mbsf)	Age (Ma)	$^{143}Nd/^{144}Nd$	Std. error (abs)	ε_{Nd} (t)	
1H	CC	7.19	0.36	0.512430	0.000004	−4.1±	0.2
5H	CC	44.89	2.47	0.512443	0.000003	−3.8±	0.1
9H	CC	83.59	5.77	0.512431	0.000009	−4.0±	0.3
9H	CC	83.59	5.77	0.512394	0.000005	−4.7±	0.2
10H	CC	91.12	7.06	0.512429	0.000004	−4.0±	0.2
10H	CC	91.12	7.06	0.512413	0.000002	−4.3±	0.1
11H	7	102.17	9.31	0.512419	0.000004	−4.2±	0.1
12H	CC	111.97	11.63	0.512398	0.000002	−4.6±	0.1
12H	CC	111.97	11.63	0.512384	0.000003	−4.8±	0.1
13H	CC	121.37	13.69	0.512383	0.000002	−4.8±	0.1
13H	CC	121.37	13.69	0.512378	0.000003	−4.9±	0.1
14H	CC	127.88	14.84	0.512452	0.000002	−3.5±	0.1
15H	CC	139.64	17.49	0.512412	0.000004	−4.2±	0.2
15H	CC	139.64	17.49	0.512411	0.000003	−4.2±	0.1

Table 3
Site U1438 Nd Isotope Data From Detrital Alumino-Silicates

Core	Section	Depth (mbsf)	Age (Ma)	$^{143}Nd/^{144}Nd$	Std. error (abs)	ε_{Nd} (t)	
12H	CC	111.97	11.63	0.512070	0.000016	−11.1±	0.6
14H	CC	127.88	14.84	0.512459	0.000004	−3.5±	0.1
16H	CC	148.96	20.40	0.512077	0.000011	−10.7±	0.4

leached in 14 ml of 0.02 M hydroxylamine hydrochloride (HH) in 20% acetic acid buffered to a pH of 4. The samples in HH solution were placed on a rotary shaker and left for 2 hr. Once the samples were leached, they were centrifuged, the supernatant decanted into a separate clean tube and centrifuged for an additional 1 hr, then decanted and dried. The samples were digested in concentrated HNO_3 overnight and then placed in 2 N HNO_3 for column chemistry.

Given the presence of disseminated ash throughout the sediment sequence, we also analyzed a few, targeted samples to characterize the detrital sediment (alumino-silicate fraction) Nd isotopic composition. The detrital silicate fraction was taken from the remaining material once the supernatant was decanted. These were placed back in HH for 1.5 hr and rinsed 3 times with Milli-Q before being left for 4 hr in HH. The samples were then rinsed 3 times with Milli-Q and dried overnight. The dried samples were homogenized and placed in 23 M HF for ~5 days until completely digested. They were dried down and placed in concentrated HNO_3-HCl-HNO_3 before finally being placed in 2 N HNO_3 in preparation for column chemistry.

All samples were then dissolved in 500 μL of 2 N HNO_3. The rare Earth elements (REEs) were isolated using Tru Spec column chemistry (isolating the REE suite from the bulk sample) and the samples collected with 3 ml of 0.05 N HNO_3 in Teflon beakers and dried down. The samples were then dissolved in 200 μL of 0.18 N HCl and placed on a 100°C hotplate overnight. The Nd fraction was isolated from the bulk REE via Ln Spec column chemistry by sequentially separating out the bulk REE. Once dried down, the remaining Nd portion was loaded onto a degassed rhenium filament (0.76 mm width, 25 μm thickness) using 1 μL of 2 N HCl and analyzed on a Thermo Scientific Triton thermal ionization mass spectrometer as Nd+. The ion beams analyzed ranged from 1 to 10×10^{-11} A, depending on the amount of Nd loaded and geometry of the double filament assembly, which was not tightly controlled (Pin et al., 2014). A run consisted of blocks of 16, each block cycled 8 times (collecting individual measurements), and a background measurement every 2 blocks; the gain was recalibrated after every 5 blocks. External precision was 15 ppm (2σ) with a value of 0.512104 based upon analysis of JNdi-1 standard (n = 34). Samples were only used if the absolute error was $<10^{-6}$. Values higher than this were discarded, with the exception of 7HCC; the ε_{Nd} errors of these samples were all within acceptable range (Tables 1–3). Several duplicates (from different samples) were run throughout to ensure reproducibility.

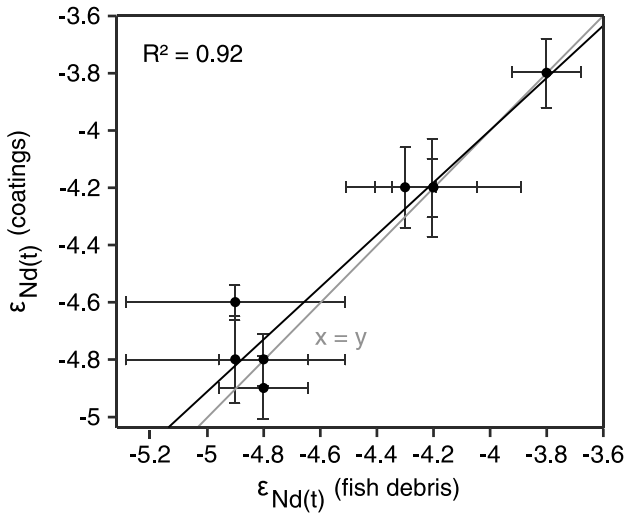

Figure 4. Comparison of ε_{Nd}(t) from fossil fish teeth and of Fe-Mn oxyhydroxide coatings in the same samples.

2.4. Calculation of ε_{Nd}(t)

The ε_{Nd} (t) values were calculated using the age model of Site U1438 (Arculus, Ishizuka, Bogus, & Expedition 351 Scientists, 2015) and representative $^{147}Sm/^{144}Nd$ values. For fish teeth/debris ε_{Nd}(t), a $^{147}Sm/^{144}Nd$ value of 0.131 was used (e.g., Thomas, 2004). Based on the average Fe-Mn crust values in Ling et al. (1997), a $^{147}Sm/^{144}Nd$ value of 0.115 was used for the Fe-Mn oxide coatings. A $^{147}Sm/^{144}Nd$ value of 0.109 was used for the detrital silicate ε_{Nd}(t) values established from upper crustal average concentrations of Sm and Nd (Taylor & McLennan, 1985). The fish teeth/debris and Fe-Mn coating values were plotted together when they were analyzed from the same sample and show similar values (R^2 = 0.92; Figure 4).

3. Results and Discussion

3.1. Isotope Values and Potential Ash Influence

The ε_{Nd} values (Tables 1 and 2) at Site U1438 fluctuated from −3.4 to −4.2 between 15 and 23 Ma, before dropping by 1.2 ε units to −4.7 by 14 Ma (Figure 5). Over the next 9 Ma, ε_{Nd} values exhibit modest

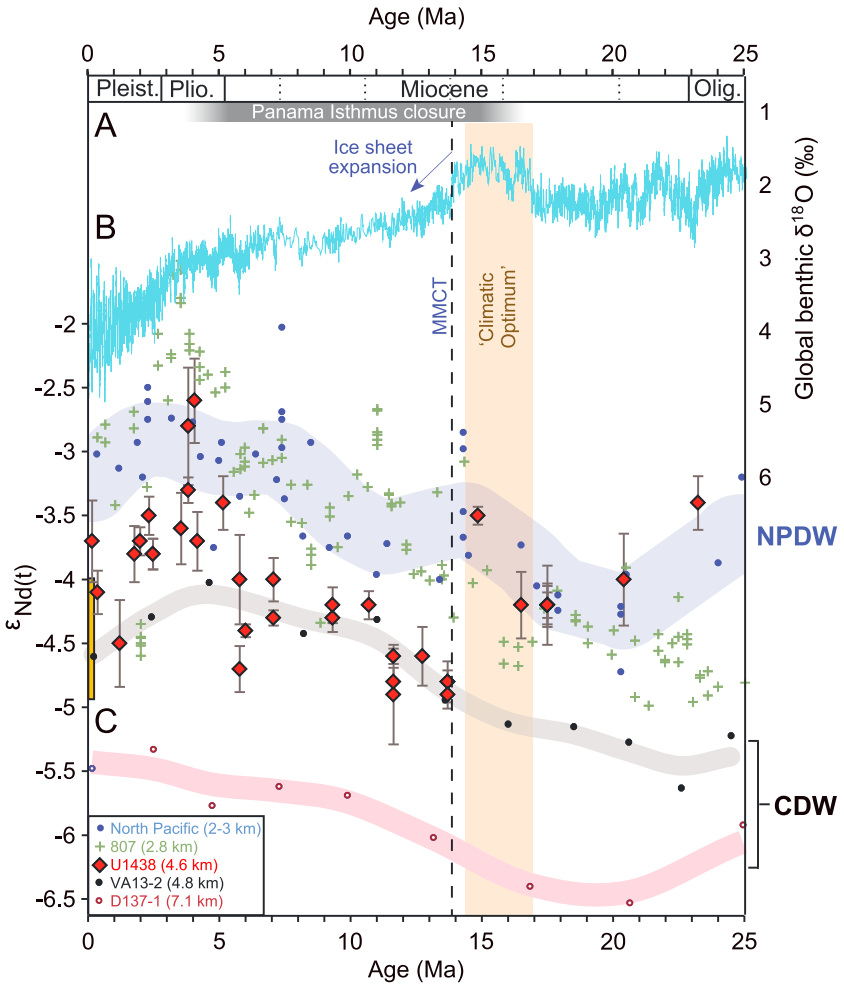

Figure 5. Summary of Philippine Sea Site U1438 ε_{Nd} data (red diamonds; 4.7-km water depth; this study) against other records. (a) Approximate time period over which the Isthmus of Panama closed is after Duque-Caro (1990). (b) The global deep ocean benthic foraminiferal oxygen isotope composite (Zachos et al., 2001). (c) Various ε_{Nd} data from Circumpolar Deep Water equatorial Pacific sites D137–1 (lower pink circles with 2-point smoothing spline; van de Flierdt et al., 2004) and VA13–2 (middle black circles with 2-point smoothing spline; Ling et al., 1997); North Pacific Deep Water North Pacific sites D11–1 (Ling et al., 1997), CD29–2 (Ling et al., 1997) and 786A (Martin & Haley, 2000; upper blue dots with 5-point smoothing spline); and equatorial Pacific Site 807A (green crosses; Le Houedec et al., 2016). The yellow bar indicates modern seawater ε_{Nd} at 5-km water depth from West Pacific sites LM-2, LM-6/11 (Amakawa et al., 2009). The Miocene "climatic optimum" is shown as a vertical orange bar during minima in Neogene deep ocean oxygen isotopes, and the middle Miocene climate transition (MMCT) is shown as a vertical dashed line at 13.8 Ma (Zachos et al., 2001).

variability (±0.5 units) and show a gradual long-term increase to −4. From 5 Ma toward the most recent samples, long-term ε_{Nd} values increase to around −3.5 but show greater variability ranging between −2.7 and −4.5 units. The highest values occur in the Pliocene at ~4 Ma.

The active eruptive phase of the proximal and extinct proto-Izu-Bonin volcanic arc—the Kyushu-Palau Ridge (Figure 1a)—had ended by the late Oligocene (Arculus, Ishizuka, Bogus, Gurnis, et al., 2015; Ishizuka et al., 2011), as evidenced at Site U1438 by the lithological change from Unit I to II (Figure 2) and the drastic change in sedimentation rate. We regard it as unlikely that upward flow of pore waters from the underlying >1-km-thick volcaniclastic sediment package (Units II to IV; see Arculus, Ishizuka, Bogus, & Expedition 351 Scientists, 2015), deposited by the active proto-Izu-Bonin arc, could have been extensive. Pore water chemistry results show the boundary between Units I and II (at 160 mbsf; Figure 2) is a very low-permeability clay-rich layer (Arculus, Ishizuka, Bogus, & Expedition 351 Scientists, 2015). However, background Neogene volcanism within the Philippine Sea region had the potential to contribute sedimentary radiogenic Nd to

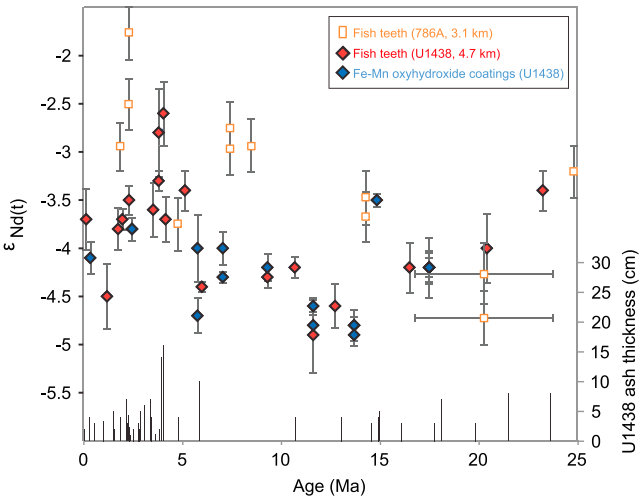

Figure 6. The ε_{Nd}(t) of fish teeth and Fe-Mn oxyhydroxide coatings from Philippine Sea sites U1438 (this study) and nearby 786A (Martin & Haley, 2000), compared with ash layers from U1438. Note that none of the samples from U1438 (this study) was taken directly at ash layers.

Site U1438 through ash. Although we avoided sampling the discrete ash layers at our site (37 ash beds over 23 Ma; Figure 6), studies have shown that dispersed ash occurs in deepwater sites east of the Izu-Bonin Arc (Scudder et al., 2014; Figure 1a). Dispersed ash in Unit I could hypothetically have impacted the Nd signal of the fish debris and Fe-Mn coatings by either postdepositional authigenic growth in ash-rich pore waters (Martin & Haley, 2000), ash-rich pore water migration into oceanic bottom waters (Abbott et al., 2015; Martin & Haley, 2000), or through oceanic exchange with dissolving dust or volcanic sediments on the seafloor (Wilson et al., 2013). The water column ε_{Nd} profile in the Oregon Basin, NE Pacific (black symbols, Figure 7a), has been argued as partially controlled by upward flux of pore fluids (Abbott et al., 2015), a process that could account for the positive offset of these (and samples from the Gulf of Alaska; white symbols, Figure 7a) from values more typical of the North Pacific (pink shading, Figure 7a). Although Site U1438 in the Philippine Sea is more distal from the continental shelf (~400 km) than these marginal sites, there is the possibility that pore water ash could impact bottom water ε_{Nd} values. However, ε_{Nd} values at Site U1438 over the last 24 million years are mostly lower than either the Gulf of Alaska or Oregon Basin (red symbols, Figure 7a) and more in line with typical water values at 4.7 km depth from a range of stations in the North Pacific. There is, however, a need for future pore water studies on NW Pacific margin sediments and water and at depths greater than 3 km.

To consider the Nd isotopic composition of the alumino-silicate fraction (and hence any potential ash that might contribute dissolved Nd to the pore waters or overlying bottom waters), we measured the alumino-silicate component of several targeted samples in the middle Miocene section of most significant change (Table 3). The extracted alumino-silicate fractions from samples at 11.63, 14.85, and 20.4 Ma have ε_{Nd} values of −11.1, −3.5, and −10.7, respectively (triangles in Figure 7b). These values generally reflect continental weathering inputs (possibly dust from East Asia) with the exception of −3.5, which indicates a proportion of andesitic-type sediment. While the alumino-silicate value of −3.5 is similar to the fish tooth analysis recorded at this interval, it is much lower than the sediment (and pore water) values at the Oregon margin (ranging from −2 to 0; Abbott et al., 2015) considered necessary to positively offset bottom waters by ~1 ε unit from typical Pacific values at those depths (−3.5 to −3). Therefore, if the fish tooth sample at 14.85 Ma was controlled by radiogenic sediment and associated pore water flux, we would expect to see an alumino-silicate fraction value higher than the fish teeth value.

Overall, the ε_{Nd} of sediment from ash-rich deposits proximal to volcanic island arc centers of the North Pacific is much higher (most commonly ranging from −2 to +8 ε units; Figure 7b) than our alumino-silicate samples. The range of ε_{Nd} values at U1438 is more typical of Pacific deepwater compositions (box-and-whisker plot, Figure 7b), indicating an overriding water mass control on the fish teeth samples at U1438. This lack of evidence for a large ash influence at U1438 is also indicated by the broadly similar values and trends recorded at nearby Site 786 (Martin & Haley, 2000; Figures 1 and 6), which is also far lower than for typical Pacific volcanic margin sediments (Figure 7b) and Oregon Margin sediments and pore waters. The most radiogenic values occur in the Pliocene interval, which does coincide with the greatest number of discrete ash layers (Figure 6), and we cannot with our data discount a volcanic ash influence here. However, these elevated Pliocene values are also seen at distal Site 807 (Le Houedec et al., 2016; Figures 1 and 5) and so we suggest they may be reflecting changing seawater values in the West Pacific region. Although hot spot activity in the Philippine Sea (e.g., Benham Rise; Figure 3) had ended by 35 Ma (Ishizuka et al., 2013), we cannot rule out the influence of volcanic activity in that region.

3.2. Water Mass Changes During the Neogene

When compared with other available data from Pacific Ocean sites (Figure 5), with no clear ash influence (from comparison with ash-rich zones, Figure 7), our results from U1438 signify likely changing deepwater sources to the Philippine Sea as the predominant control on ε_{Nd} values. North Pacific sites from ~10 to

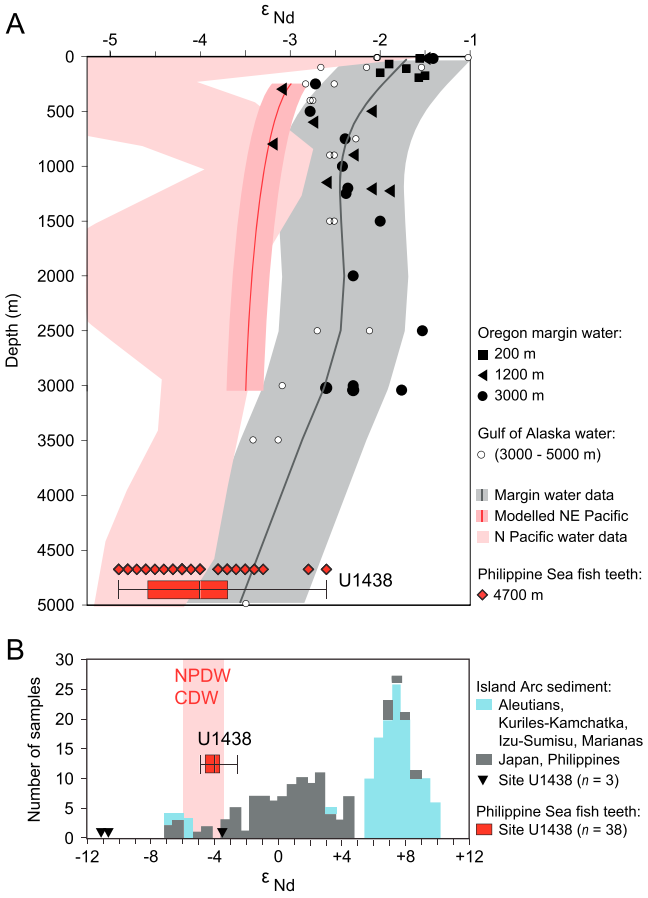

Figure 7. The ε_{Nd} (t) of fish teeth and Fe-Mn oxyhydroxide coatings from Site U1438 (this study) compared with various modern North Pacific Ocean water and sediment samples. (a) Modern water sample ε_{Nd} data (black symbols, with 7-point black smoothing spline and ±1σ gray area) from the marginal Gulf of Alaska (Haley et al., 2014) and Oregon margin (Abbott et al., 2015). Data show a significant positive offset from NE Pacific modeled seawater (dark pink zone; Abbott et al., 2015) and from measured NW and NE Pacific seawater (light pink zone; sites BO-3, BO-5, LM-2, LM-6/11, TPS 24 271-1, and TPS 24 76-1; Amakawa et al., 2009). Site U1438 data, spanning the last 24 Ma, largely sit within the expected range of seawater. (b) Modern ε_{Nd} values for sediment collected close to island arcs (Jones et al., 1994), considered influenced by radiogenic volcanic material. The ε_{Nd} (t) of fish teeth and Fe-Mn oxyhydroxide coatings from Site U1438 (red box-and-whisker), and detrital alumino-silicates (black triangles), do not show a strong radiogenic signal, but rather a typical range for intermediate and deep North Pacific seawater (shown as pink bar).

30°N (Ling et al., 1997; Martin & Haley, 2000) at intermediate NPDW depths (ranging from 1.8 to 3.1 km) exhibit generally higher radiogenic values over the past 25 Ma, with averages from −4 to −3 (Figure 5c). Equatorial Pacific Site 807 is monitoring a more southerly extent of NPDW today (2.8 km), and its greater variability (averages from −4.5 to −2.5) has been interpreted as due to alternating contributions of Upper CDW and NPIW (Le Houedec et al., 2016). We observe the majority of the Site 807 record from 25 Ma to Recent overlaps with NPDW end member values (Figure 5), although some of the less radiogenic values may not represent pure NPDW. Equatorial Pacific Site VA13-2 (4.8 km water depth; Ling et al., 1997), which does monitor CDW today (Figure 8a), exhibits relatively less radiogenic values with ε_{Nd} ranging from −5.5 to −4 (Figure 5). Finally, Equatorial Pacific Site DC137-01 (van de Flierdt et al., 2004), at an abyssal depth of 7.2 km and most impacted by CDW today (Figure 8a), shows the least radiogenic ε_{Nd} values ranging from −6.5 to −5.5 since 25 Ma (Figure 5).

With the Neogene evolution of Pacific intermediate and deepwater mass values thus constrained (Figure 5), the ε_{Nd} results from U1438 can be seen as indicating changes in the relative contribution of CDW to the deep Philippine Sea. Before ~14.8 Ma (Figure 8c), Site U1438 was bathed in local intermediate NPDW (ε_{Nd} values closer to intermediate water), and between ~13.7 Ma and present (Figure 8b), CDW penetrated further northward into the deep North Pacific, lowering ε_{Nd} values. Our results therefore indicate a major deep ocean reorganization occurred in the Pacific Ocean between 14.8 and 13.7 Ma. This ε_{Nd} shift of >1 is comparable to the 1.5 ε unit shift of NPDW in the North Pacific during the Paleogene, interpreted as caused by local deepwater formation (Thomas, 2004). The Philippine Sea Plate modest 6° of latitude gradual movement northward away from the CDW source over the last 20 Ma (Figure 3) could not explain the negative ε_{Nd} changes at Site U1438, as this movement would have distanced Site U1438 from the less radiogenic southern-sourced water mass.

3.3. Tectonic Influences

Between ~15 and 23 Ma, our results show that, remarkably, the deep NW Pacific (>4.7 km) was bathed in NPDW (Figure 8c), not CDW as it was after 14 Ma (Figure 8b) and as it is today (Figure 8a). Ocean circulation modeling by Butzin et al. (2011) and von der Heydt and Dijkstra (2006) shows that a continental configuration change from the Oligocene to Miocene, which included a more restricted Isthmus of Panama (Figure 5a) and less redistribution through the Tethys circumequatorial flow, caused North Pacific overturning to become more limited and southern component deepwater to penetrate further northward into the Pacific. Thus, if this modeling is correct, it is possible that the enhanced CDW flux since 14 Ma was the result of restricted Atlantic high salinity inflow, and lower North Pacific salinity causing stifled North Pacific overturning. However, if this process does explain the gradual increase in both deep and intermediate Pacific Ocean water ε_{Nd} (e.g., Martin & Haley, 2000), it is then less able to explain the abrupt evolution of Site U1438 ε_{Nd} values as they show a different trend to other sites (Figure 5). This leads us to favor nontectonic processes for the increased CDW flux to the Philippine Sea in the middle Miocene.

Another significant tectonic change impacting the Pacific, the closure of the Indonesian Gateway by 14 Ma (Gourlan et al., 2008), prevented the flow of less radiogenic water (ε_{Nd} below −7) into the Pacific and could thus have resulted in a trend toward more radiogenic values in the Pacific. Therefore, this gateway closure could not have directly caused the negative ε_{Nd} shift at U1438. We note, however, that it is possible the

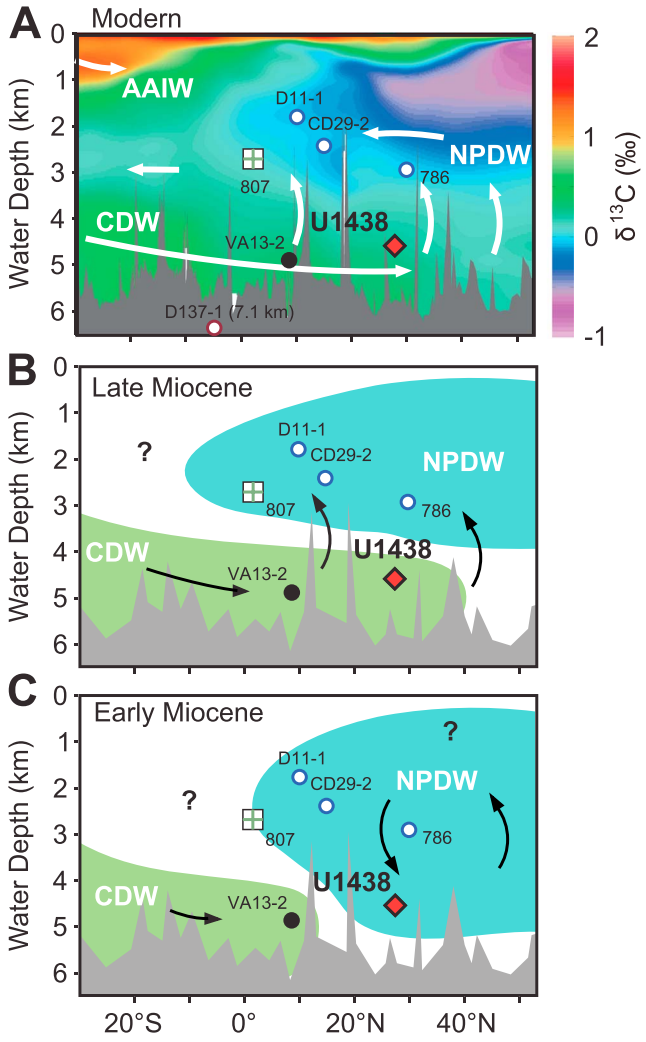

Figure 8. Pacific Ocean profiles through time, with locations of major water masses and sites discussed in the text. (a) Modern Pacific Ocean seawater $\delta^{13}C$ profile (based on GLODAP data set; Key et al., 2004), overlaid with modern ocean deepwater currents and water masses modified from Kawabe and Fujio (2010), and the position of core sites discussed in the text. (b) Schematic representing water mass structure in the Pacific Ocean after the middle Miocene climate transition at ~14 Ma. (c) Before ~14 Ma. NPDW: North Pacific Deep Water; CDW: Circumpolar Deep Water; AAIW: Antarctic Intermediate Water.

diversion of Indian Ocean deepwater southward around Australia (Gourlan et al., 2008) could have had some unconstrained influence on source waters for CDW. In the West Pacific, Le Houedec et al. (2016) hypothesize irregular seafloor tectonic reorganization to explain the pseudo cyclic 7–11 Ma variations in ε_{Nd} at Site 807 from 35 Ma onward. If tectonic variations did occur, they may have controlled the rate of margin volcanism in the West Pacific. Although our record is of lower resolution than 807, there are similar changes to U1438 from 14 Ma onward (Figure 5), in particular a positive excursion in the Pliocene, which may be indicative of greater margin activity around the Philippine and Japan margins (Le Houedec et al., 2016). However, as the relatively abrupt negative ε_{Nd} shift to Site U1438 at ~14 Ma is counter to the more positive NPDW records (including Site 807), regional margin activity does not appear to be a plausible cause of the less radiogenic shift at ~14 Ma.

3.4. Antarctic Glaciation at 13.8 Ma

We conclude that the rather abrupt appearance of CDW in the Philippine Sea between 14.8 and 13.7 Ma could not have been caused by gradual tectonic closure of the Isthmus of Panama or the closure of the Indonesian Gateway (which would have elevated West Pacific ε_{Nd} values). An alternative explanation is Antarctic glaciation at 13.8 Ma, increased deepwater formation around Antarctica, and increased export of CDW further north into the Pacific. The approximate temporal coincidence of increased CDW flux to the Philippine Sea with the rapid (<100 ka) ice sheet build up on East Antarctica and sea level fall (Lear et al., 2010) at the MMCT (Figure 5) indicates that greater production of CDW may have resulted from Antarctic processes, although we acknowledge that higher resolution records are needed to test this temporal link. Greater production of CDW in the Southern Ocean during the MMCT was interpreted from increased glacial offsets in $\delta^{18}O$ with depth at various sites east and west of New Zealand (Flower & Kennett, 1995), and significantly strengthened overturning circulation in the Southern Ocean during the MMCT was modeled from sea level fall, ice sheet growth, and CO_2 reduction (Huang et al., 2017). In that study, Antarctic ice sheet growth, declining temperatures, and a greater extent of sea ice particularly in the Ross and Weddell Seas promoted AABW formation during the MMCT (Huang et al., 2017). Despite no change in ε_{Nd} at equatorial Pacific intermediate sites over the MMCT, and a modest positive shift in anomalously unradiogenic intermediate water in the South China Sea (Ma et al., 2018), Holbourn et al. (2013) suggested that enhanced benthic $\delta^{13}C$ gradients between Pacific intermediate and deep sites were caused by an invigorated PMOC at 13.8 Ma and that increased benthic $\delta^{18}O$ offsets were caused by cooling NPDW. In the context of our new ε_{Nd} data, the rapidity of these $\delta^{13}C$ and $\delta^{18}O$ changes and approximate coincidence with the MMCT (Holbourn et al., 2013) suggests that the CDW expansion detected at Site U1438 was possibly caused by enhanced CDW formation and northward flux in response to Antarctic glaciation since the MMCT, the largest Antarctic climate switch of the past 25 Ma.

4. Conclusions

New Nd isotopic data from IODP Site U1438 in the Philippine Sea (4.7 km water depth) provide the first constraints on the evolution of deep water in the abyssal North Pacific over the Neogene. Although there is a need for future studies of NW Pacific marginal marine sediments and pore waters near volcanic centers, comparisons with available ε_{Nd} data from these settings, and from open Pacific sites, suggest that

changing ocean water values rather than pore waters were the principal driver of the data set. Our results indicate that the water source for the deep Philippine Sea remained relatively stable for the majority of the last 23 Ma, as ε_{Nd} values follow the gradual trends that are present in both intermediate and deepwater sites in the Pacific Ocean attesting to its long term stratification. The gradual increase toward more radiogenic values in all Pacific intermediate and deep sites from ~15 to ~5 Ma may be due to a gradual decline in Atlantic Ocean inflow through a closing Isthmus of Panama (Martin & Haley, 2000). However, a unique change in ε_{Nd} at Site U1438, expressed as a secular drop of 1 ε unit compared to other Pacific sites, occurred between 14.8 and 13.7 Ma which signifies a likely northward expansion of CDW into the abyssal Philippine Sea. It is possible that a stifled inflow of saline Atlantic water through a restricting Isthmus of Panama reduced North Pacific surface water salinity and inhibited local deepwater formation. However, the coincidence of this increased northward flux of CDW with global cooling and ice sheet expansion at the MMCT (13.8 Ma) could be explained by enhanced formation of CDW source waters in a cooling Southern Ocean (Huang et al., 2017) causing a greater flow of CDW into the deep North Pacific. Higher temporal resolution records from other North Pacific sites are now required to constrain the timing and extent of this expanded CDW flow. A smaller change in our records occurred at 5 Ma, with a 0.5 ε unit increase that is mirrored in West Pacific Site 807, and could be a regional radiogenic water mass signal or possibly the coincidental influence of dispersed ash. Our records suggest that PMOC responded to the most significant long-term climate change event of the Neogene. By contrast, outside of this interval, PMOC appears to have been relatively stable, within the resolution and sensitivity of the records, for much of the Neogene. Our results have implications for future studies aiming to constrain global carbon cycle changes over the MMCT, as an increased carbon-rich CDW flux to the deep North Pacific may have replaced local NPDW ventilation before 14 Ma.

Acknowledgments
We thank the IODP for providing core material and the captain, crew, and technical staff of the *JOIDES Resolution* who sailed on Expedition 351. This work was funded by the Natural Environment Research Council (NERC) grant RGS 114419 to S.K. We thank Jun Tian and an anonymous reviewer for providing helpful comments on the manuscript. The data supporting this publication can be obtained from the tables. The bulk of the shipboard-collected data from this expedition is accessible from the IODP *JOIDES Resolution* Science Operator, Texas A&M University (TAMU), at http://www.iodp.tamu.edu/database/index.html.

References

Abbott, A. N., Haley, B., & McManus, J. (2015). Bottoms up: Sedimentary control of the deep North Pacific Ocean's ε_{Nd} signature. *Geology*, *43*(11), 1035–1038. https://doi.org/10.1130/G37114.1

Amakawa, H., Sasaki, K., & Ebihara, M. (2009). Nd isotopic composition in the central North Pacific. *Geochimica et Cosmochimica Acta*, *73*(16), 4705–4719. https://doi.org/10.1016/j.gca.2009.05.058

Arculus, R. J., Ishizuka, O., Bogus, K., & Expedition 351 Scientists (2015). Proceedings of the International Ocean Discovery Program, Expedition 351: Izu-Bonin-Mariana Arc Origins. College Station, TX (International Ocean Discovery Program). doi:https://doi.org/10.14379/iodproc. 351.2015

Arculus, R. J., Ishizuka, O., Bogus, K. A., Gurnis, M., Hickey-Vargas, R., Aljahdali, M. H., et al. (2015). A record of spontaneous subduction initiation in the Izu–Bonin–Mariana arc. *Nature Geoscience*, *8*(9), 728–733. https://doi.org/10.1038/ngeo2515

Arsouze, T., Dutay, J.-C., Lacan, F., & Jeandel, C. (2007). Modeling the neodymium isotopic composition with a global ocean circulation model. *Chemical Geology*, *239*, 165–177.

Bartoli, G., Sarnthein, M., Weinelt, M., Erlenkeuser, H., Garbe-Schönberg, D., & Lea, D. W. (2005). Final closure of Panama and the onset of northern hemisphere glaciation. *Earth and Planetary Science Letters*, *237*(1-2), 33–44. https://doi.org/10.1016/j.epsl.2005.06.020

Basak, C., Martin, E. E., & Kamenov, G. D. (2011). Seawater Pb isotopes extracted from Cenozoic marine sediments. *Chemical Geology*, *286*(3), 94–108.

Butzin, M., Lohmann, G., & Bickert, T. (2011). Miocene Ocean circulation inferred from marine carbon cycle modeling combined with benthic isotope records. *Paleoceanography*, *26*, PA1203. https://doi.org/10.1029/2009PA001901

De Paolo, D. J., & Wasserburg, G. J. (1976). Nd isotopic variations and petrogenetic models. *Geophysical Research Letters*, *3*, 249–252. https://doi.org/10.1029/GL003i005p00249

Duque-Caro, H. (1990). Neogene stratigraphy, paleoceanography and paleobiogeography in Northwest South America and the evolution of the Panama seaway. *Palaeogeography, Palaeoclimatology, Palaeoecology*, *77*(3-4), 203–234. https://doi.org/10.1016/0031-0182(90)90178-A

Ferrari, R., Jansen, M. F., Adkins, J. F., Burke, A., Stewart, A. L., & Thompson, A. F. (2014). Antarctic Sea ice control on ocean circulation in present and glacial climates. *Proceedings of the National Academy of Sciences of the United States of America*, *111*(24), 8753–8758. https://doi.org/10.1073/pnas.1323922111

Flower, B. B., & Kennett, J. P. (1995). Middle Miocene deepwater paleoceanography in the southwest Pacific: Relations with East Antarctic ice sheet development. *Paleoceanography*, *10*, 1095–1112. https://doi.org/10.1029/95PA02022

Gourlan, A. T., Meynadier, L., & Allegre, C. J. (2008). Tectonically driven changes in the Indian Ocean circulation over the last 25 Ma: Neodymium isotope evidence. *Earth and Planetary Science Letters*, *267*(1-2), 353–364. https://doi.org/10.1016/j.epsl.2007.11.054

Haley, B. A., Frank, M., Hathorne, E., & Pisias, N. (2014). Biogeochemical implications from dissolved rare Earth elements and Nd isotope distributions in the Gulf of Alaska. *Geochimica et Cosmochimica Acta*, *126*, 455–474. https://doi.org/10.1016/j.gca.2013.11.012

Holbourn, A., Kuhnt, W., Frank, M., & Haley, B. A. (2013). Changes in Pacific Ocean circulation following the Miocene onset of permanent Antarctic ice cover. *Earth and Planetary Science Letters*, *365*, 38–50. https://doi.org/10.1016/j.epsl.2013.01.020

Huang, X., Starz, M., Gohl, K., Knorr, G., & Lohmann, G. (2017). Impact of Weddell Sea shelf progradation on Antarctic bottom water formation during the Miocene. *Paleoceanography*, *32*, 304–317. https://doi.org/10.1002/2016PA002987

Ishizuka, O., Taylor, R. N., Ohara, Y., & Yuasa, M. (2013). Upwelling, rifting, and age-progressive magmatism from the Oki-Daito mantle plume. *Geology*, *41*(9), 1011–1014. https://doi.org/10.1130/G34525.1

Ishizuka, O., Taylor, R. N., Yuasa, M., & Ohara, Y. (2011). Making and breaking an island arc: A new perspective from the Oligocene Kyushu-Palau arc, Philippine Sea. *Geochemistry, Geophysics, Geosystems*, *12*, Q05005. https://doi.org/10.1029/2010GC003440

Jones, C. E., Halliday, A. N., Rea, D. K., & Owen, R. M. (1994). Neodymium isotopic variations in North Pacific modern silicate sediment and the insignificance of detrital REE contributions to seawater. *Earth and Planetary Science Letters*, *127*(1-4), 55–66. https://doi.org/10.1016/0012-821X(94)90197-X

Kaneko, I., Takatsuki, Y., & Kamiya, H. (2001). Circulation of intermediate and deep waters in the Philippine Sea. *Journal of Oceanography*, *57*(4), 397–420. https://doi.org/10.1023/A:1021565031846

Kawabe, M., & Fujio, S. (2010). Pacific Ocean circulation based on observation. *Journal of Oceanography*, *66*(3), 389–403. https://doi.org/10.1007/s10872-010-0034-8

Key, R. M., Kozyr, A., Sabine, C. L., Lee, K., Wanninkhof, R., Bullister, J. L., et al. (2004). A global ocean carbon climatology: Results from Global Data Analysis Project (GLODAP). *Global Biogeochemical Cycles*, *18*, GB4031. https://doi.org/10.1029/2004GB002247

Le Houedec, S., Meynadier, L., & Allègre, C. J. (2016). Seawater Nd isotope variation in the western Pacific Ocean since 80 Ma (ODP 807, Ontong Java Plateau). *Marine Geology*, *380*, 138–147. https://doi.org/10.1016/j.margeo.2016.07.005

Lear, C. H., Mawbey, E. M., & Rosenthal, Y. (2010). Cenozoic benthic foraminiferal Mg/Ca and Li/Ca records: Towards unlocking temperatures and saturation states. *Paleoceanography*, *25*, PA4215. https://doi.org/10.1029/2009PA001880

Ling, H. F., Burton, K. W., O'Nions, R. K., Kamber, B. S., von Blanckenburg, F., Gibb, A. J., & Hein, J. R. (1997). Evolution of Nd and Pb isotopes in Central Pacific seawater from ferromanganese crusts. *Earth and Planetary Science Letters*, *146*(1-2), 1–12. https://doi.org/10.1016/S0012-821X(96)00224-5

Ma, X., Tian, J., Ma, W., Li, K., & Yu, J. (2018). Changes of deep Pacific overturning circulation and carbonate chemistry during the middle Miocene East Antarctic ice sheet expansion. *Earth and Planetary Science Letters*, *484*, 253–263. https://doi.org/10.1016/j.epsl.2017.12.002

Martin, E. E., & Haley, B. A. (2000). Fossil fish teeth as proxies for seawater Sr and Nd. *Geochimica et Cosmochimica Acta*, *64*(5), 835–847. https://doi.org/10.1016/S0016-7037(99)00376-2

Pälike, H., Lyle, M. W., Nishi, H., Raffi, I., Ridgwell, A., Gamage, K., et al. (2012). A Cenozoic record of the equatorial Pacific carbonate compensation depth. *Nature*, *488*(7413), 609–614. https://doi.org/10.1038/nature11360

Reynard, B., Lècuyer, C., & Grandjean, P. (1999). Crystal-chemical controls on rare-earth element concentrations in fossil biogenic apatites and implications for paleoenvironmental reconstructions. *Chemical Geology*, *155*(3-4), 233–241. https://doi.org/10.1016/S0009-2541(98)00169-7

Pin, C., Dupont, A., & Gannoun, A. (2014). Rapid, simultaneous separation of Sr, Pb, and Nd by extraction chromatography prior to isotope ratios determination by TIMS and MC-ICP-MS. *Journal of Analytical Atomic Spectrometry*, *29*(10), 1858–1870. https://doi.org/10.1039/c4ja00169a

Richter, C., & Ali, J. R. (2015). Philippine Sea Plate motion history: Eocene-recent record from ODP Site 1201, central west Philippine Basin. *Earth and Planetary Science Letters*, *410*, 165–173. https://doi.org/10.1016/j.epsl.2014.11.032

Scudder, R., Murray, R. W., Schindlbeck, J. C., Kutterolf, S., Hauff, F., & McKinley, C. C. (2014). Regional-scale input of dispersed and discrete volcanic ash to the Izu-Bonin and Mariana subduction zones. *Geochemistry, Geophysics, Geosystems*, *15*, 4369–4379. https://doi.org/10.1002/2014GC005561

Tachikawa, K., Athias, V., & Jeandel, C. (2003). Neodymium budget in the modern ocean and paleo-oceanographic implications. *Journal of Geophysical Research*, *108*(C8), 3254. https://doi.org/10.1029/1999JC000285

Talley, L. (2013). Closure of the global overturning circulation through the Indian, Pacific, and Southern Oceans: Schematics and transports. *Oceanography*, *26*(1), 80–97. https://doi.org/10.5670/oceanog.2013.07

Talley, L. T., Pickard, G. L., Emery, W. J., & Swift, J. H. (2011). *Descriptive physical oceanography: An introduction, 6 Ed*. Elsevier, Boston, Mass: Academic Press.

Taylor, S. R., & McLennan, S. M. (1985). The continental crust, its composition and evolution: An examination of the geochemical record preserved in sedimentary rocks. Oxford; Boston: Blackwell Scientific; Palo Alto, Calif.: Fistributors, USA and Canada, Blackwell Scientific.

Thomas, D. J. (2004). Evidence for production of North Pacific Deep Waters during the early Cenozoic greenhouse. *Nature*, *430*(6995), 65–68. https://doi.org/10.1038/nature02639

Thomas, D. J., Korty, T., Huber, M., Schubert, J. A., & Haines, B. (2014). Nd isotopic structure of the Pacific Ocean 70–30 Ma and numerical evidence for vigorous ocean circulation and ocean heat transport in a greenhouse world. *Paleoceanography*, *29*, 454–469. https://doi.org/10.1002/2013PA002535

van de Flierdt, T., Frank, M., Halliday, A. N., Hein, J. R., Hattendorf, B., Günther, D., & Kubik, W. (2004). Deep and bottom water export from the Southern Ocean to the Pacific over the past 38 million years. *Paleoceanography*, *19*, PA1020. https://doi.org/10.1029/2003PA000923

von der Heydt, A., & Dijkstra, H. A. (2006). Effect of ocean gateways on the global ocean circulation in the late Oligocene and early Miocene. *Paleoceanography*, *21*, PA1011. https://doi.org/10.1029/2005PA001149

Wilson, D. J., Piotrowski, A. M., Galy, A., & Clegg, J. A. (2013). Reactivity of neodymium carriers in deep sea sediments: Implications for boundary exchange and paleoceanography. *Geochemica et Cosmochemica Acta*, *109*, 197–221. https://doi.org/10.1016/j.gca.2013.01.042

Wu, J., Suppe, J., Lu, R., & Kanda, R. (2016). Philippine Sea and East Asian plate tectonics since 52 Ma constrained by new subducted slab reconstruction methods. *Journal of Geophysical Research: Solid Earth*, *121*, 4670–4741. https://doi.org/10.1002/2016JB012923

Xie, R. C., Marcantonio, F., & Schmidt, M. W. (2012). Deglacial variability of Antarctic Intermediate Water penetration into the North Atlantic from authigenic neodymium isotope ratios. *Paleoceanography*, *27*, PA3221. https://doi.org/10.1029/2012PA002337

Zachos, J., Pagani, M., Sloan, L., Thomas, E., & Billups, K. (2001). Trends, rhythms, and aberrations in global climate 65 Ma to present. *Science*, *292*(5517), 686–693. https://doi.org/10.1126/science.1059412